Unsaturated out-of-plane permeability measured with three-dimensional flow monitoring by etched fiber sensors

Xiao Liu[a,b*], Pedro Sousa[b], Helge Pfeiffer[b], Xinlin Qing[d], Stepan V. Lomov[b], Jan Ivens[c]

[a]*School of Information Engineering, Wuhan University of Technology, Wuhan 430070, China*

[b]*Department of Materials Engineering, KU Leuven, Kasteelpark Arenberg 44, BE-3001 Leuven, Belgium*

[c]*Department of Materials Engineering, KU Leuven–Campus De Nayer, J. De Nayerlaan 5, B-2870 Sint-Katelijne Waver, Belgium*

[d]*School of Aerospace Engineering, Xiamen University, Xiamen 361005, China*

*Corresponding author, email: yijieguoke@outlook.com

Abstract

In our work, the three-dimensional flow in stacks of biaxial E-glass fiber non-crimp fabrics (NCF), unidirectional carbon fiber layers, and multiaxial carbon fiber NCF is monitored by the etched fiber sensors embedded inside the fabric stack. The sensors diameter is 200 μm; the influence of the sensor embedding on the flow is experimentally illustrated and discussed. For three materials with known in-plane permeability, a radial infusion model was adopted for the calculation of the out-of-plane permeability. Based on this, the assumed radius of the semi-ellipsoidal flow was fitted to provide an easier way. The paper verifies these two methods for the case of a non-negligible radius of injection tube compared to the thickness of samples and demonstrated the uncertainties related to the unknown flow pattern near the inlet. The results open a way for further development and normalization of the embedded sensors method for the out-of-plane permeability measurement.

Keywords

B. Permeability; B. Porosity; D. Process monitoring; E. Resin flow.

1. Introduction

For the Liquid Composite Molding (LCM) process, the common defects that occur during the filling process are dry spots or resin rich areas caused by uneven resin impregnation. These problems cannot be easily corrected because trial-and-error approaches are inefficient and costly [1]. That is why numerical simulations are frequently used to analyze resin flow and to assess process design to ensure complete saturation of the textile reinforcement. Based on Darcy's law, the permeability of fibrous preforms is a decisive input parameter for simulation-based predictions of common defects, which should be determined experimentally [2].

The permeability tests can be divided into two categories: saturated and unsaturated tests. The saturated tests normally measure the ratio between steady state flow rate and pressure drop in flow of a chosen fluid through an already saturated fabric reinforcement, with the flow towards chosen directions. They are quite different from the real unsaturated LCM process where the advancing flow front is an important feature of the process [3]. The unsaturated tests, which are discussed in this work, are closer to the nature of a real-world LCM process.

The unsaturated permeability can be determined only if the flow front position is measured in real-time. For the in-plane permeability, the radial flow experiment can measure principal permeability components K_x, K_y and the orientation of the principal coordinate system β in one test. In the test procedure used in the benchmark exercise [4] and stipulated by the standard [5], the test fluid is injected under constant injection pressure through a central injection gate into a tool cavity containing the reinforcement sample. With the progressive flow front obtained visually, the approach developed by

Weitzenböck et al [6,7] is used in this paper to acquire the prior knowledge of in-plane permeability.

Measurement of permeability in the out-of-plane direction can be more challenging than the in-plane due to the difficulty to determine the invisible flow front along the thickness direction with the shorter distance of travel of the fluid. A benchmark exercise of out-of-plane permeability measurement for reinforcement textiles had been carried out by 26 institutions, the results showed a variability of two orders of magnitude between participants [8]. A majority of participants used a 1D saturated test method while a few selected a 1D unsaturated or a 3D unsaturated flow method.

Due to the difficulty to monitor the real-time flow front in thickness direction, there are few relevant papers about the out-of-plane permeability of unsaturated three-dimensional flow test, especially for a thick fiber stack. The flow front monitoring techniques can be divided into two categories: non-intrusive methods and embedded sensors. For non-intrusive methods, Nedanov and Advani [9] employed a video camera to capture the point when the resin reached the bottom layer and the approximate intermediate positions of the flow through the thickness were determined using the mass measured by an electronic balance. Yun et al [10] recorded the movement of the 2D flow front of the resin with two digital cameras and then coupled it to an optimization algorithm and flow simulation tool to identify the full permeability tensor. For another non-intrusive method, ultrasonic sensors with the assumption of constant sound velocity within dry and wet preforms are applied. So, the flow front along thickness direction and the time of flight of ultrasonic longitudinal wave are linearly correlated. Based on this, Stöven et al [11] addressed the monitoring of three-dimensional ellipsoidal impregnation induced by point injection and the through-the-thickness

permeability was determined by a numerical flow simulation software. Becker et al [12] and Konstantopoulos et al [13] presented the unsaturated out-of-plane permeability measurement systems with the method of the functional determination of the inlet radii. Textile-induced inhomogeneities and varying measurement parameters, e.g., injection pressure, were found to be main reasons for the deviations.

For non-intrusive methods, the real-time flow front is calculated indirectly based on assumptions, which will lead to errors compared with direct measurement methods using embedded sensors. Weitzenböck et al [14] used thermistors placed at different locations through the depth and width of the mould lay-up. The optical fiber is light-weight, minimally intrusive, compatible with conductive (carbon) fiber and a non-transparent mold. Based on the Fresnel reflection, Antonucci et al [15] used the optical fiber to obtain the three-dimensional resin front location by detecting the reflected optical signal at the end of the fiber. Ahn et al [16] and Lim et al [17] used etched fiber sensor with small cladding segments removed to detect the local flow front. Principal permeability directions and values are calculated from the ellipsoidal resin flow front in 3D. Results from the optic sensor measurements were compared with the radial flow technique and a good correlation was found.

The embedded sensors will inevitably affect the flow front. Another problem is that many researches mentioned above neglected the size of injection tube and the point injection assumption was adopted for easier calculation. In the present paper we tackle these two problems.

Based on the experimental fact that the in-plane flow would be severely disturbed by the etched fiber sensor (EFS) embedded inside, we test the in-plane and out-of-plane permeabilities separately, i.e., the in-plane flow front was monitored by a camera and the invisible through-thickness flow front was tracked by the EFS in two series of tests.

Even with the injection tube of non-negligible size, the accurate out-of-plane permeability can be determined with the knowledge of in-plane permeabilities using the radial infusion model developed by Mekic [18]. Then the best fit of the coefficient, the ratio between the assumed radius of the hemispherical flow r_0 and the radius of injection tube R_0, is calculated at different injection pressures, which provides an easier way for the calculation of the out-of-plane permeability. The experimental method with good repeatability and stability is established to determine the out-of-plane permeability under unsaturated three-dimensional flow.

2. Methodology

2.1 Flow front tracking

An optical fiber consisting of silica core, polymer cladding and Tefzel coating is used, as shown in Fig.1. A small segment of 1-2 mm length of the coating can be removed by a soldering iron with the advantage of low temperature and size control. Then the cladding could be removed by fast burn or chemical soaking. By this method, multiple etched areas are made on one optical fiber.

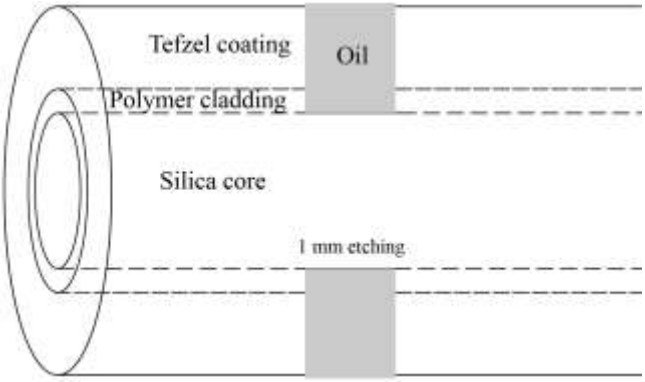


Fig.1 The schematic diagram of etched fiber sensor

Before injection, the EFS is embedded into the textile reinforcement and exposed to air, the reflection coefficient was 0.036. When the oil covers the EFS, the coefficient dropped to 0.00219, as shown in Table.1. The light leaks into the liquid and this results in the loss of light power, more etched areas result in more losses. The time points at

which the signals begin to decrease are extracted and used as the time of arrival of the flow front.

Table.1 Reflection coefficient of different medias

media	**refraction index** n	**reflection coefficient** $\boldsymbol{R = (\frac{n_1-n_2}{n_1+n_2})^2}$	
Air	1	0.0346	---
Silica core	1.457		0.00219
Oil	1.6	---	

For each through-thickness test, one optical fiber consisting of four EFSs is placed right below the injection hole to obtain four data points of through-thickness flow fronts vs. injection times, as shown the in the Fig.2 ($z_{f1} - z_{f4}$ of yellow points). Each sensor loop has $n/5$ fabric layers in between and n is the total number of layers. The corresponding flow front locations along the thickness direction are calculated by averaging the total thickness, so we have $z_{fi} = \frac{i}{5}h, i \leq 5$. The last data point was obtained by the camera: as soon as the flow front could be seen from the camera, the injection time should be noted (z_{f5} of green point). Therefore, the EFS could be used as a multi-point flow sensor which can track the flow front in-situ.

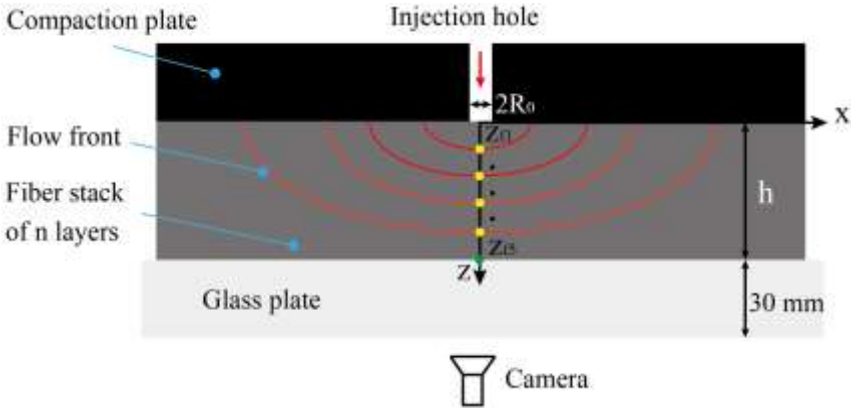
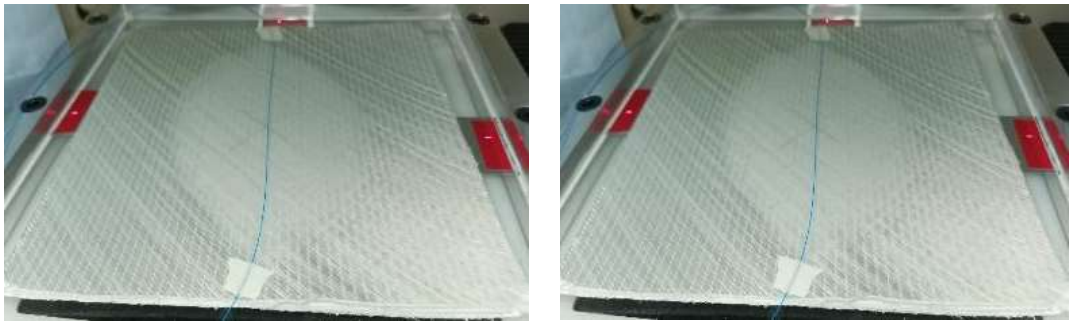


Fig.2 The schematic diagram of experimental setup

The optical fibers are fragile and their installation is an acknowledged tricky problem. Paralleled placement in different layers of fiber stack is a common installation method for EFS. However, preliminary tests indicated that a race tracking channel was introduced where the oil flowed faster along the fiber, which had a big impact on the

in-plane flow front, as shown in Fig.3. In contrast, the flow in the thickness direction would be hardly disturbed because the EFS is only placed in between a limited number of layers. Therefore, it was decided to track the in-plane and through-thickness flow front by camera and EFS, respectively and separately.



(a) EFS on the 10th layer (b) EFS on the 15th layer

Fig.3 The in-plane flow front disrupted by EFS (the size of the mould is 350 mm × 350 mm)

2.2 Out-of-plane permeability calculation

Once the through-thickness flow fronts at different time steps are tracked, the out-of-plane permeability can be calculated in different ways, as shown in Table.2. Based on Darcy's Law, an equation for method-1 can be derived under the assumption of a semi-ellipsoidal flow close to the inlet formed by a semi-ellipsoidal injection port [16]. In practice, it is difficult to build such a special port and the injection port generally is hemi-spherical with the radius corresponding to the cylindrical pipe for liquid supply with the radius of R_0. However, a closed form solution cannot be obtained for a perform with a hemi-spherical injection port. So, the semi-ellipsoidal inlet radius in the z direction is fictitious as r_0, which is extremely difficult to measure directly from experiments. For convenience, $r_0 = R_0$ in Ref [16] and $r_0 = 0.1R_0$ in Ref [14].

For different materials, the final flow shape is of course different and unknown prior to the measurement. Therefore, it would be almost impossible to accurately

implement the hemi-spherical notch in the fiber preform. To solve this problem, an alternative method-2 by using the functional determination of the inlet radii is applied. The effective inlet radius is calculated by the mass of injected fluid [12,13].

However, the above-mentioned methods are not accurate because the diameter of the inlet is often comparable or even larger than the thickness of a thin fabric preform. To overcome this, a radial infusion model had been developed by Mekic [18] and the analytic solution can be obtained by using a nonlinear transformation into oblate ellipsoid coordinate system, as shown in method-3. When the thickness of the preform is much larger than the diameter of circular opening, approximating the point source solution, the method-3 can be reduced into the asymptotic form as method 4 which we also list it for comparison.

Table.2 Equations used in 3D unsaturated flow experiments

Method	Pros and Cons
1. $K_z = \frac{\eta\varepsilon}{6\Delta p}[\frac{2z_f^3}{r_0} - 3z_f^2 + {r_0}^2]\frac{1}{t}$ η: viscosity of liquid; ε: porosity Δp:the pressure gradient between inlet and flow front z_f: flow front along the thickness direction r_0: fictitious semi-ellipsoidal inlet radius in the z direction R_0:the inlet radius t: time during the injection	For $r_0 = R_0$, a hemi-spherical notch needed to be made on the surface of the preform [16]; In Ref [14], $r_0 = 0.1R_0$ because the initial flow front is disc shaped (rather than hemi-spherical) and should be much smaller than the radius of the inlet.
2. $K_z = (\frac{z_f}{r_f})^2 \frac{\eta\varepsilon}{6\Delta pt}[\frac{2z_f^3}{{r_{02}}^2} - 3z_f^2 + {r_{02}}^2]$ where $r_f = (\frac{3m}{2\pi\rho\varepsilon})^{1/3}, r_{02} = R_0\sqrt{\frac{z_f}{r_f}}$ r_f: flow front position in equivalent isotropic coordinates m: mass of injected fluid ρ: density of injected fluid r_{02}: effective inlet radius	The mass of injected fluid needed to be monitored and only values greater 6 mm flow front height could be considered [12,13].
3. $F\left(\xi_f, \frac{\pi}{2}\right) = \frac{K_{xye}\Delta p}{{R_0}^2\eta\varepsilon}t, z_f = \sqrt{\frac{K_z}{K_{xye}}}R_0\sinh(\xi_f)$ $F(\xi_f, \pi/2) = F_1(\xi_f) + F_2(\xi_f)$ $F_1(\xi_f) = \frac{1}{6}\left\{(4\arctan e^{\xi_f} - \pi)\sinh^3\xi_f - \frac{1}{2}(\cosh 2\xi_f - 1) + 2\ln\cosh\xi_f\right\}$ $F_2(\xi_f) = \frac{1}{2}\left\{(4\arctan e^{\xi_f} - \pi)\sinh^3\xi_f - 2\ln\cosh\xi_f\right\}$	Need to know the in-plane permeability values, they can be used even if the diameter of the inlet is comparable or larger than the thickness of a fabric preform [18].

ξ_f: curvilinear coordinate describing flow front K_{xye}: equivalent in-plane permeability, $K_{xye} = \sqrt{K_x K_y}$		
4.	$z_f = \sqrt{\frac{K_z}{K_{xye}}}[\frac{6K_{xye}\Delta p R_0}{\pi\eta\varepsilon}t]^{1/3}$	The asymptotic form of Method-3

For the analytical solution, they are accurate with the necessary prior knowledge of in-plane permeabilities, which require really high material and labor cost especially for thick carbon fiber preforms. In order to find an easier way to calculate the out-of-plane permeability for the case of a non-negligible radius of injection tube compared to the thickness of samples, the assumed radius of the semi-ellipsoidal flow in the z direction needs to be determined theoretically and experimentally. For a thick sample, when the flow front is far from the injection tube and the details about source geometry are ignored, the formulas are presented as follows:

$$c = \frac{K_z}{K_{xye}},\ z_f = c^{1/3} R_f \tag{1}$$

$$\frac{1}{3}(\frac{R_f}{R_{\mathrm{ps}}})^3 - \frac{1}{2}\left(\frac{R_f}{R_{\mathrm{ps}}}\right)^2 + \frac{1}{6} = \frac{K_e \Delta p}{\eta\varepsilon R_{\mathrm{ps}}^2} t \tag{2}$$

$$K_e = \left(K_z K_{xye}^2\right)^{1/3} = c^{1/3} K_{xye} \tag{3}$$

where c is the anisotropy characterization of out-of-plane and in-plane equivalent permeability; R_{ps} is the characteristic size of a point source that is assumed to have spherical shape after the original transversely orthotropic media being converted into isotropic media with the effective permeability K_e.

After combining the Eq. (1)-(3), we can get：

$$K_z = (2\frac{z_f^3}{R_{ps} c^{1/3}} - 3z_f^2 + {R_{ps}}^2 c^{2/3})\frac{\eta\varepsilon}{6\Delta p t} \tag{4}$$

The Eq. (1)-(3) can be reduced when $z_f \gg R_{ps}$[18], which corresponds to the developed phase of the liquid spreading process:

$$z_f = c^{1/3}(\frac{3K_e \Delta p R_{\mathrm{ps}}}{\eta\varepsilon} t)^{1/3} \tag{5}$$

The displacement ratio between the two asymptotic solutions of method 4 and Eq. (5) is:

$$\frac{z_f^{(method-4)}}{z_f^{(Eq.5)}} = c^{1/18}\left(\frac{2R_0}{\pi R_{\mathrm{ps}}}\right)^{1/3} \tag{6}$$

To get the best fit of these two solutions, the assumed R_{ps} should be:

$$R_{ps} = \frac{2}{\pi} R_0 c^{1/6} \tag{7}$$

Thus, the Eq. (8) can be derived by introducing the Eq. (7) into Eq. (4):

$$K_z = \left(\pi \frac{z_f^3}{R_0 c^{1/2}} - 3z_f^2 + \frac{4}{\pi^2} R_0^2 c\right) \frac{\eta \varepsilon}{6 \Delta p t} \tag{8}$$

The assumed radius of the semi-ellipsoidal flow in the z direction of method-1 can be accurately defined as:

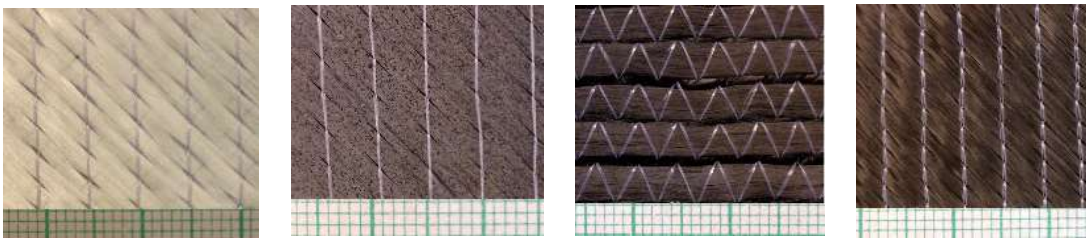
$$r_0 = \frac{2}{\pi} c^{1/2} R_0 \tag{9}$$

The Eq. (8) can be used to calculate the out-of-plane permeability with the experimental results of through-thickness flow front positions z_f at different injection times and the anisotropy characterization c. The calculation method will be verified by using the materials with known in-plane permeability.

3. Experiment setup

3.1 Materials

Three kinds of fabrics, a biaxial E-glass non-crimp fabric (NCF-E glass), a NCF unidirectional carbon fabric (NCF-UD45) and a NCF multiaxial carbon fabric (NCF-M) were employed here. Scissors are used to cut out specimens and each layer is aligned carefully. The images are shown in Fig.4 (a)-(d). The stacking sequence, areal density of the fabrics and volume density of the fibres are listed in Table.3.



(a) NCF-E glass (b) NCF-UD45 (c) NCF-M top (d) NCF-M bottom

Fig.4 The images of three kinds of fabrics

Table.3 Material properties of three kinds of fabrics

Fiber	**Stacking sequence**	**Areal density-** A_w $(\mathrm{g/m^2})$	**Volume density-** ρ $(\mathrm{kg/m^3})$
Biaxial non-crimped E-glass fabric	[-45°/+45°]	450	2550
NCF C-PLY SP UD45 100 C3	[-45°]	100	1750
NCF Multiaxial carbon fiber	[0°/-45°/90°/+45°]	1200	1750

The permeability highly depends on the fiber volume fraction (FVC), and three target fiber volume fractions are needed for the tests by a well-designed number of layers and the thickness of each fabric, as shown in Table.4 calculated by the equation $V_f = \frac{A_w n}{h\rho}$. The dimensions of all square samples are 250 mm ×250 mm to achieve the same boundary conditions.

As for the tested liquid, the Dow Corning ® Xiameter PMX 200/100 cS which is widely used in the benchmark exercise of permeability measurement is selected [4,8]. The ARES-G2 rheometer from TA Instruments was used to obtain the viscosity-temperature curve at a representative shear rate of 100 1/s and the result is shown in Fig.5. The temperatures at different locations: in the pressure vessel, the oil, the environment and inside the sample before and after injection are monitored. The difference in temperature is within 4℃. The temperature inside the sample is used and the viscosity for each single test is calculated using the viscosity-temperature curve.

Table.4 Specimen details for three fiber volume fractions V_f

Materials	**Number of layers-n**	**Injection pressure** Δp (bar)	**Thickness-h** (mm)	**FVCs-V_f**	**Dimensions** (mm^2)
E-glass	25	0.4	7.25	60.8%	250×250
		0.4	7.95	55.5%	
		0.4	8.79	50.2%	
NCF-UD45	60	3.1	6.59	52.0%	
		1.0	7.15	48.0%	
		0.5	7.92	43.3%	
NCF-M	15	0.45	16.06	64.8%	
		0.45	16.66	61.5%	
		0.45	18.12	57.4%	

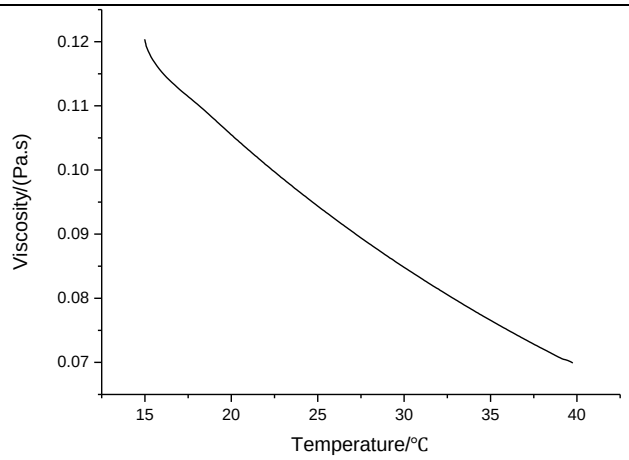
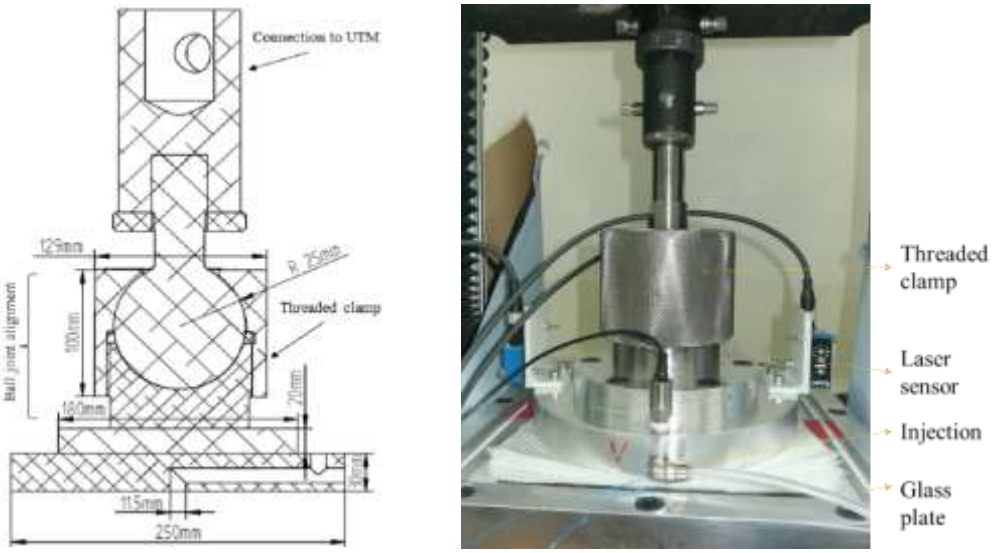


Fig.5 The viscosity vs temperature curve of Dow Corning used in this study

3.2 Fabric compaction

In order to compress the fabric to a certain thickness and inject the oil from the center, a universal testing machine (UTM) with a special designed compaction system is used. As shown in Fig.6 (a), the compaction system includes a head connected to the UTM, the self-alignment ball joint, the threaded clamp and the compaction plate with one central injection hole. Three laser sensors are installed on the top surface of the compaction plate, see Fig.6 (b), which allow to measure the parallelism of the compaction plate, as well as the thickness of the preform directly. When two out of the three laser sensors reach the set thickness, the compaction process will stop automatically.



(a) cross-section view (b) experiment image

Fig.6 The special designed compaction system

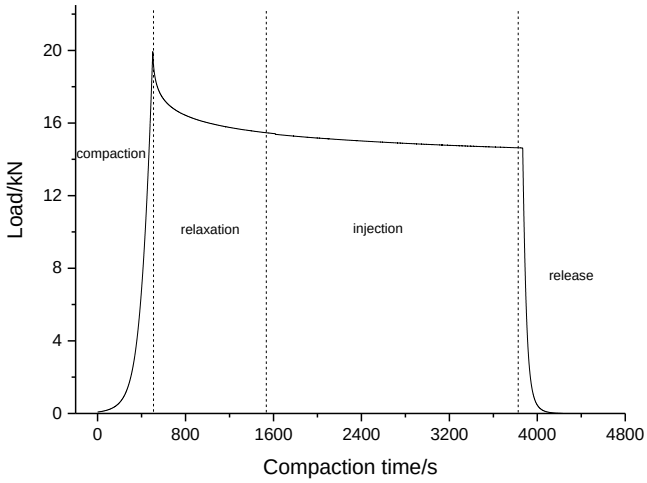


Fig.7 A typical load curves during one entire permeability test from UTM

A typical load curve during one entire permeability test from UTM is shown in Fig.7, there are four steps for each test. Correspondingly, the experiment process is as follows:

1. Compaction: prepare the aligned sample with and without the EFS sensor placed and then compress it to designed thickness;
2. Relaxation: hold the load and wait ten minutes for relaxation;
3. Injection: inject oil and monitor the flow front with EFS or camera in real time;

4. Release: close the injection and release the sample.

3.3 Etched fiber sensor (EFS)

The multimode optical fibre from Thorlabs with a core diameter of 200 μm, 0.39 NA and low-OH is used (product name FT200EMT), which exhibits impressive performance and transmission from the Vis to NIR (400 to 2200 nm). For each test, one optical fiber consisting of four EFSs is embedded into the fiber stack. The laser source will excite red light and the power meter is connected to the end of fiber to monitor the light power in real time. The experimental setup for the 3D unsaturated permeability test is shown in Fig. 8.

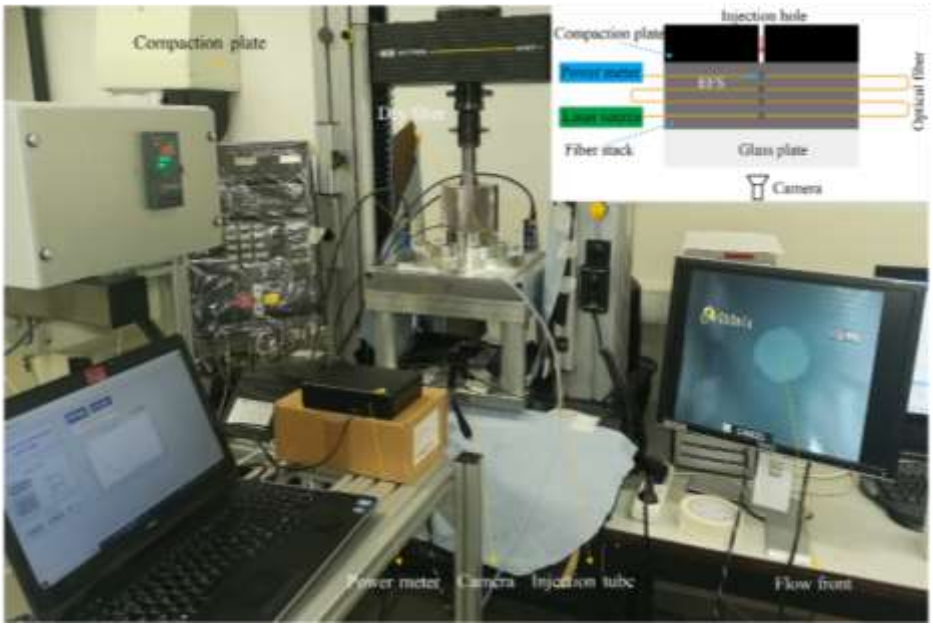
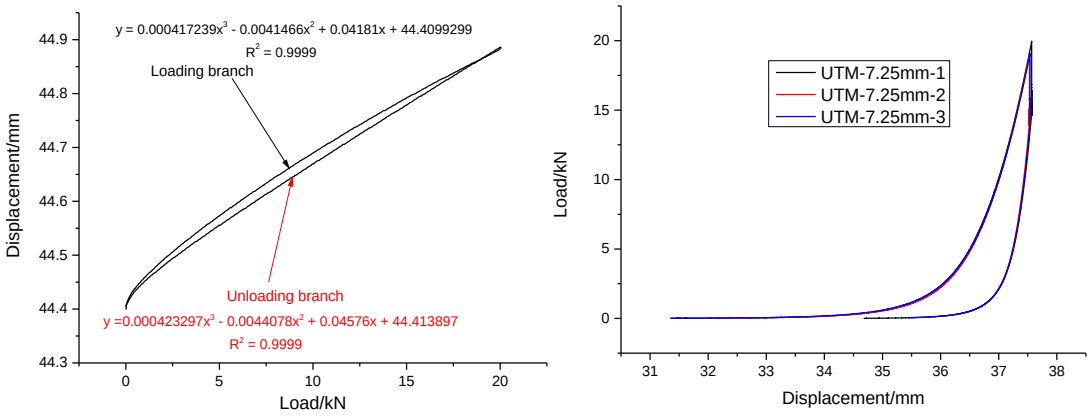


Fig.8 Experimental setup for 3D unsaturated permeability test

The camera is also used for the in-plane tests without EFS sensors. A through-thickness hole with the same size of the injection hole is made in the center of each sample for in-plane tests. The oil would fill the hole immediately and go evenly through each layer. The flow fronts at different injection times are captured at constant time step. For both in and out-of-plane tests, each test for a certain FVC is repeated at least three times. The inlet pressure is measured at the pot.

3.4 Thickness measurement

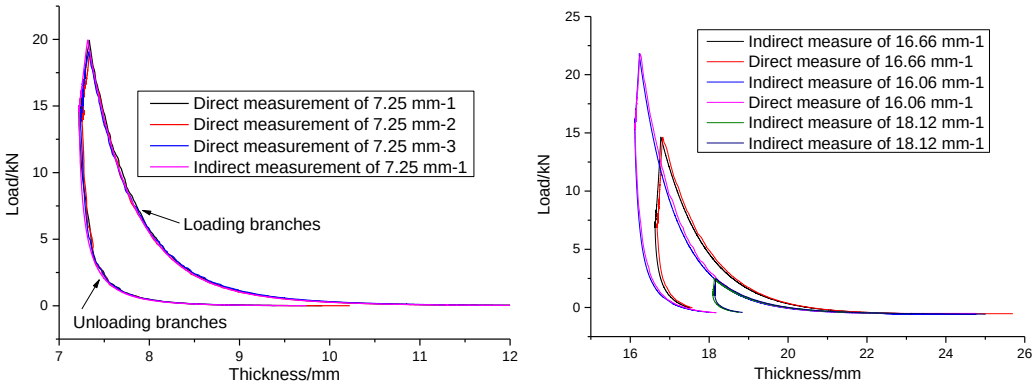
The thickness measurement method is crucial and need to be validated to ensure the target FVC. Based on our previous study [19], two thickness measurement methods are employed here including the indirect measurement by the displacement sensor of UTM and the direct measurement by the laser sensors. The indirect thickness is calculated by subtracting the approximated calibration of the loading and unloading compliance curve from the original load-displacement curves, as shown in Fig.9. And the direct thickness is calculated by averaging the values of three laser sensors.



(a) Compliance curve (b) Load-displacement curves

Fig.9 The approximated calibration of the loading and unloading compliance curve and the original load-displacement curves of one test

The thickness measurement results of NCF E-glass fabric of same thickness and of NCF multiaxial carbon fabric of different thicknesses are shown in Fig. 10. We observed that the curves of indirect and direct measurement methods overlapped well, which indicates that these two methods can be mutually verified, and the thickness of the samples can be accurately measured and controlled to meet the requirements of permeability tests.



(a) NCF E-glass fabric (b) NCF multiaxial carbon fabric

Fig.10 The comparisons of indirect and indirect thickness measurement methods

4. Glass fiber stacks

4.1 In-plane permeability tests

The in-plane tests are carried out using samples with a through-thickness hole in the center. The through-thickness hole has the same diameter as the central injection gate and two holes need to be carefully aligned to ensure the fast impregnation in the thickness direction. Then the oil flows evenly in each layer immediately and the advance of the flow front is tracked by the camera at a fixed time step. For example, the flow fronts of NCF E-glass fiber of different injection times at a time step of two seconds are shown in Fig. 11.

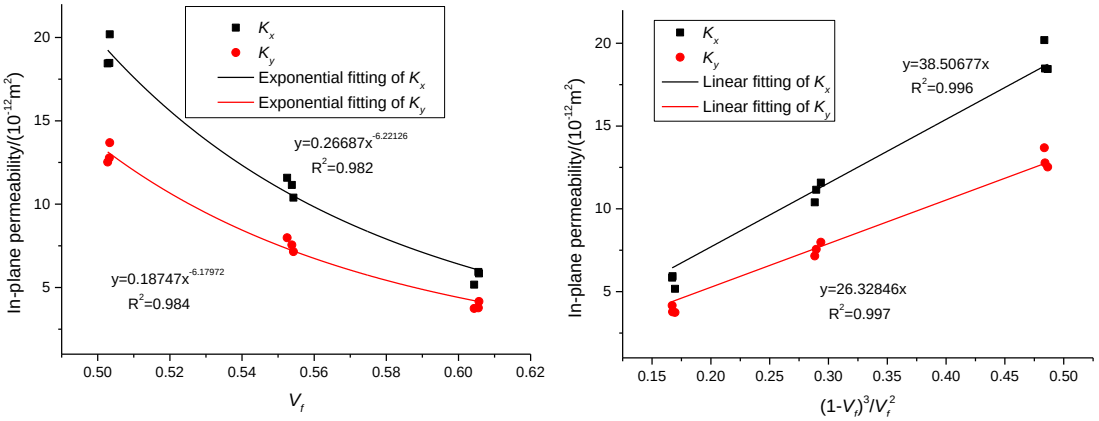


(a) 94s (b) 214 s (c) 374 s

Fig.11 The flow field of NCF E-glass fabric monitored by the camera

When the flow field at different time step is obtained, the flow fronts of three in-plane directions (0°,45°,90°) can be calculated and the method developed by Weitzenböck et al [6,7] is used. For each in-plane test, 15 data points of flow fronts are

used from the time step when a relatively regular elliptic flow front can be seen up to the time step when the flow front reaches the edge of monitoring area. The principal in-plane permeability results of NCF E-glass fabric are shown in Fig.12. The exponential fitting and Kozeny-Carman fitting are also used to approximate the dependence of the permeability of reinforcements on the V_f with the equation $K_{x,y,z} = k_0 \frac{(1-V_f)^3}{V_f^2}$. The coefficient of determination R^2 indicates a very good quality of each fit.



(a) exponential fitting (b) Kozeny-Carman fitting

Fig.12 The principal in-plane permeability results of NCF E-glass fabric

4.2 Out-of-plane permeability tests

For the out-of-plane permeability tests, the EFS is used throughout the impregnation process. The typical signals when the oil is injected into NCF E-glass fabric of 8 mm thickness are shown in Fig.13. As we can see, the normalized voltage of light of each test has very consistent trends: the voltage decreases at four similar times due to the leak of light when the oil arrives four EFS; the voltage decreases very fast at the first two EFS and slowly at the last two EFS because the oil flows much slower at latter times. As indicated in Section 2.1, five data points of injection times (t) and flow fronts along the thickness direction (z_f) can be obtained for each test.

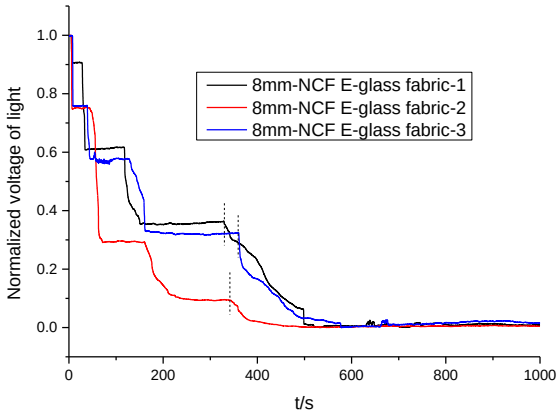


Fig.13 Typical EFS signals of NCF E-glass fabric tests at 8 mm thickness

With the values of in-plane permeabilities, the method 3 of the Table. 2 can be used to get the exact solution of out-of-plane permeabilities. Based on the point source approximation, the method 4 of Table. 2 and the Eq. (8) are also used and compared. Three methods are re-arranged as Eq. (10-12). As soon as the left and right sides of the equations are determined, the slopes can be obtained by using a linear fit through the origin and the out-of-plane permeabilities can be calculated.

$$z_f/R_0 = \sqrt{\frac{K_z}{K_{xye}}}\sinh(\xi_f) \tag{10}$$

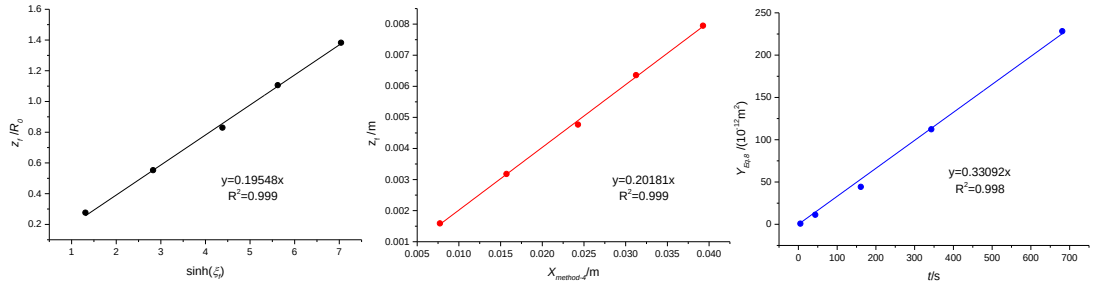
$$z_f = \sqrt{\frac{K_z}{K_{xye}}}\left[\frac{6K_{xye}\Delta p R_0}{\pi\eta\varepsilon}t\right]^{1/3} = \sqrt{\frac{K_z}{K_{xye}}}X_{method-4} \tag{11}$$

$$Y_{Eq.8} = \left(\pi\frac{z_f^3}{R_0 c^{1/2}} - 3z_f^2 + \frac{4}{\pi^2}R_0^2 c\right)\frac{\eta\varepsilon}{6\Delta p} = K_z t \tag{12}$$

Five data points of one test (8 mm-NCF E-glass fabric-2) are listed in Table. 5 and the linear fit through the origin of three out-of-plane permeability calculation methods are plotted in Fig. 14.

Table .5 Data points for 8 mm-NCF E-glass fabric-2 test

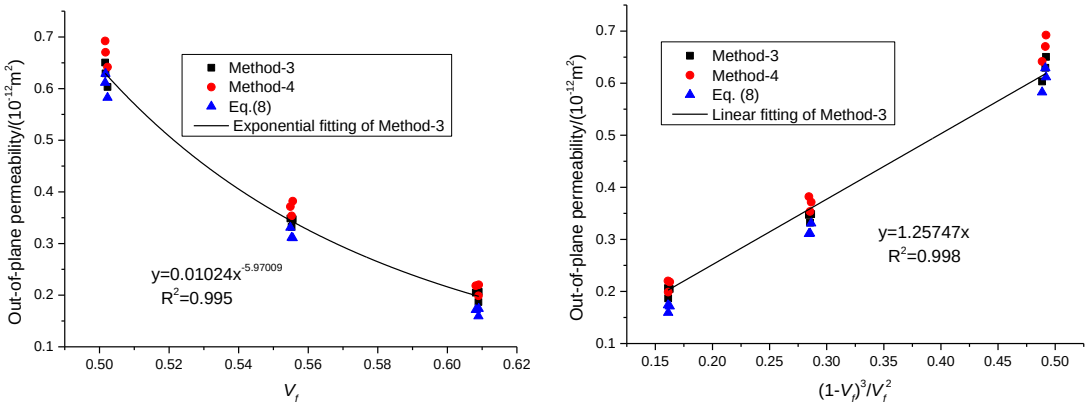
Data points	t /s	z_f /m	z_f/R_0	$\sinh(\xi_f)$	$X_{method-4}$ /m	$Y_{Eq.8}$/ (10^{-12}m^2)
1	5.2	0.00159	0.27656	1.31015	0.00773	0.78206
2	43.6	0.00318	0.55311	2.82633	0.01571	11.28107
3	161.0	0.00477	0.82967	4.380723	0.02428	44.25507
4	343.0	0.00636	1.10623	5.62137	0.03124	112.36594
5	681.0	0.00795	1.38278	7.03990	0.03927	228.27556



(a) method 3 (b) method 4 (c) Eq. (8)

Fig.14 The linear fit through the origin of 8 mm-NCF E-glass fabric-2 test

The out-of-plane permeability results of NCF E-glass fabrics of different FVCs are shown in Fig. 15. The exponential and linear fitting of Method-3 show a good result. For the point source approximation of Method-4, the injection hole is assumed to be very small, so the injection time of real test is smaller than the approximation, resulting in bigger values than the exact values of Method-3. As for Eq. (8), the values are closer to the exact values.



(a) exponential fitting (b) Kozeny-Carman fitting

Fig.15 The out-of-plane permeability results of NCF E-glass fabrics

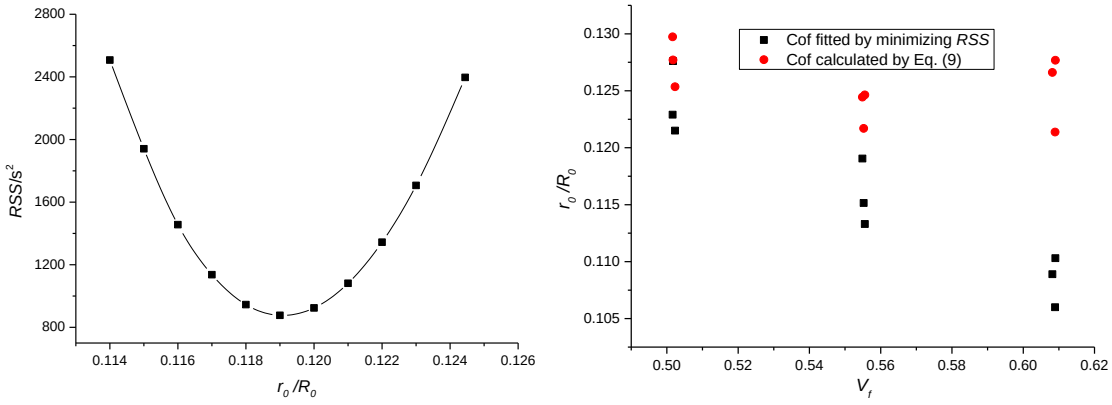
4.3 Determination of the coefficient $a = r_0/R_0$

In Eq. (8) and (9), the ratio between the assumed radius of the hemispherical flow and the radius of injection tube is: $a_{Eq.(9)} = r_0/R_0 = \frac{2}{\pi}\sqrt{\frac{K_z}{K_{xye}}}$. With the exact solution of out-of-plane permeability values k_z and the flow fronts of each test, the times when

the oil should arrive can be calculated by Eq. (13). The Residual Sum of Squares (*RSS*) of calculated times and real test times when the flow front arrives is calculated by using the Eq. (14). The best fit of the ratio $a = r_0/R_0$ can be obtained by minimizing the value of *RSS*, as shown in Fig. 16(a). The results of the fitted and calculated coefficient (Cof) are shown in Fig. 16(b). The values are quite close and all values are between 0.105 and 0.130. Theoretically, this coefficient is only related to the radius of the injection port and the anisotropy characterization c, which should be independent of V_f. However, the Cof-fitted are closer to the Cof-calculated at lower V_f and bigger thickness due to the reason that they are more consistent with the point source approximation.

$$t_{i,cal} = \frac{\eta\varepsilon}{6\Delta p}\left[\frac{2z_{f,i}^3}{aR_0} - 3z_{f,i}^2 + (aR_0)^2\right]\frac{1}{K_z} \tag{13}$$

$$RSS = \sum_{i=1}^{5}(t_{i,cal} - t_{i,test})^2 \tag{14}$$



(a) coefficient determination (b) coefficient results

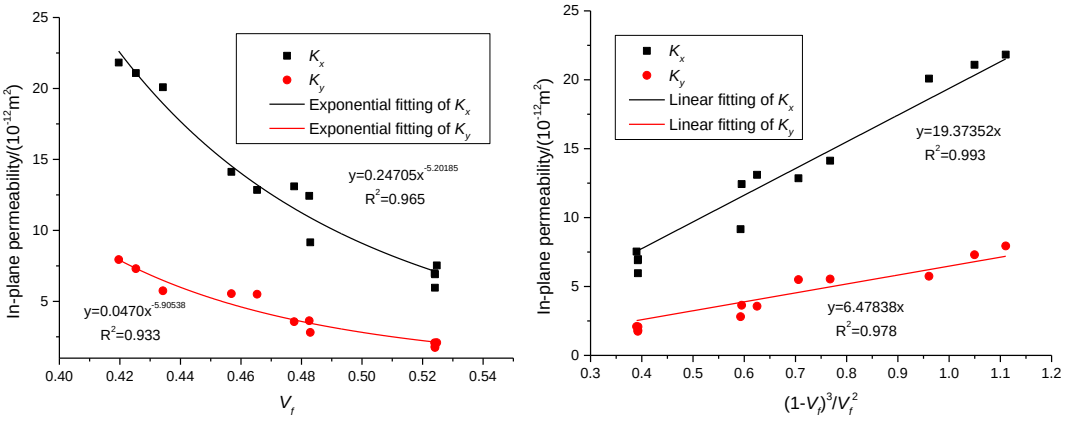
Fig.16 The determination method and results of the coefficient r_0/R_0

5. Carbon fiber stacks

5.1 Permeability tests of NCF-UD45

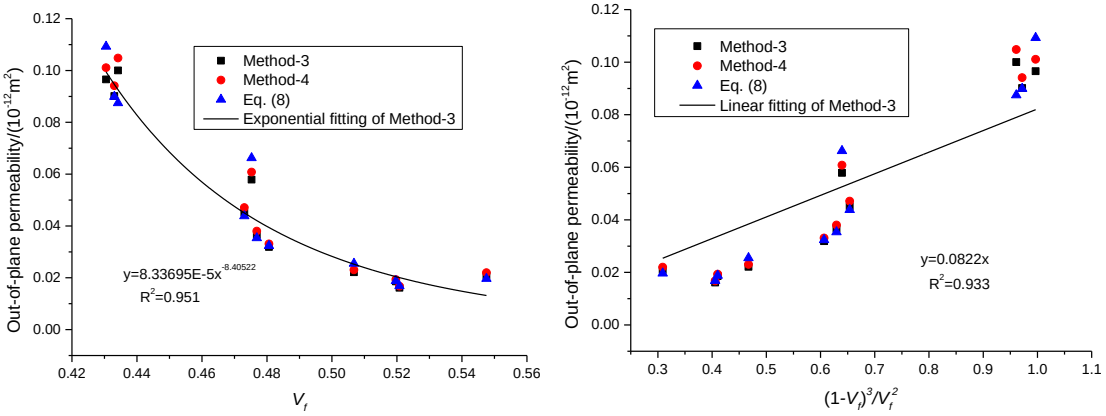
The same procedures as NCF E-glass for in-plane and out-of-plane permeability tests are used for NCF unidirectional carbon fabric. The in-plane results are shown in Fig. 17 and the out-of-plane results are shown in Fig. 18. Compared with the glass fiber

stack, the NCF-UD45 carbon fabric has lower out-of-plane permeability and anisotropy characterization c. Moreover, we see poorer linear correlation for the carbon NCF-UD45 than for the glass (Fig. 18 (b)), the reason is that the Kozeny constant is defined by the geometry of the pores in the medium, which has a substantial scatter due to the layer nesting, fiber distortion, and non-uniformities in fiber packing arrangement during the sample preparation of 60 plies [20].



(a) exponential fitting (b) Kozeny-Carman fitting

Fig.17 The principal in-plane permeability results of NCF-UD45



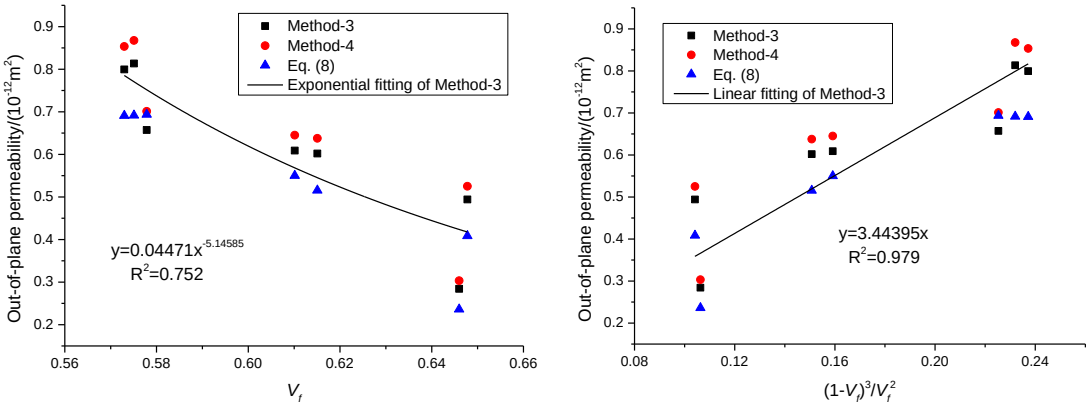
(a) exponential fitting (b) Kozeny-Carman fitting

Fig.18 The out-of-plane permeability results of NCF-UD45

5.2 *Out-of-plane permeability tests of NCF-M*

Because each layer of the NCF multiaxial carbon fabric is the same as the NCF-UD45, and the different stacking sequences don't affect the equivalent in-plane

permeability, the in-plane permeability results of NCF-UD45 can be still used here. The out-of-plane permeability results of NCF-M are shown in Fig.19 and show higher scatter than the glass fiber. Even though the data differ by a biggest factor 1.74 at V_f = 0.65, the results could be considered as satisfying regarding the softer carbon fabric is more easily distorted during manipulation and the impreciseness that can occur during the injection process.

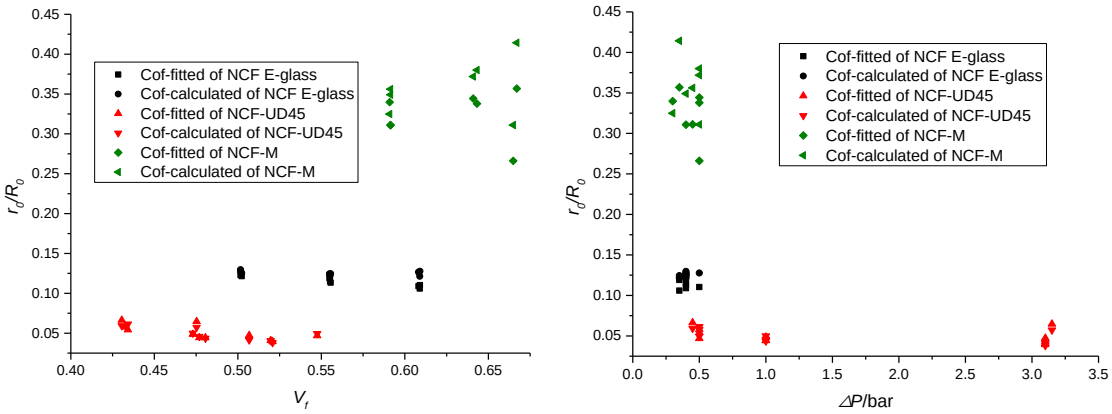


(a) exponential fitting (b) Kozeny-Carman fitting

Fig.19 The out-of-plane permeability results of NCF multiaxial carbon fabric

5.3 Determination of the coefficient $a = r_0/R_0$

The coefficients $a = r_0/R_0$ of NCF-UD45 and NCF-M are also determined and shown in Fig.20.



(a) (b)

Fig.20 The out-of-plane permeability results of NCF multiaxial carbon fabric

It can be found that the values of Cof calculated by Eq. (9) are consistent with the values of Cof fitted by minimizing *RSS*. The same trend as NCF E-glass fiber can be found that the Cof-fitted are closer to the Cof-calculated at lower V_f. And the Fig.20 (b) indicates that the coefficient is in-dependent on the injection pressure.

6. Conclusions

In our present work, the out-of-plane permeability of glass and carbon fiber stacks is measured under unsaturated three-dimensional flow with the prior knowledge of in-plane permeability. The in-plane and out-of-plane tests are carried out in two series to avoid the effect of the embedded sensors on the in-plane flow. When the through-the-thickness flow fronts at different injection times are obtained, three different permeability calculation methods including the exact solution, the point source approximation and the fictitious semi-ellipsoidal inlet radius method are used and compared, even with the injection tube of non-negligible size. The results of the carbon fabrics exhibit larger scatter and are less repeatable than the glass fabric, because the softer carbon fabric is more easily distorted during manipulation. For the point source approximation, the permeability results are always bigger than the exact values because the injection time of real test is smaller than the approximation. The permeability results of the fictitious semi-ellipsoidal inlet radius method are closer to the exact values. The ratio between the radius of fictitious semi-ellipsoidal flow and the injection tube is obtained by the best fit of the exact solution. The experimental results show that the ratio mainly depends on the anisotropy characterization, and shows no relation with the injection pressure. However, the results of the ratios are found to be more accurate at the stacks with lower V_f and bigger thickness due to the reason that these tests are more consistent with the point source approximation.

Acknowledgment

Funding: This work was supported by the China Scholarship Council and the National Natural Science Foundation of China (Grants No. 11972314). The author would also like to acknowledge Johan Vanhulst, Bart Pelgrims and Kris Van de Staey at Department of Materials Engineering of KU-Leuven for their technical supports.

References

[1] Khoun L, Palardy G, Hubert P. Relation between volumetric changes of unsaturated polyester resin and surface finish quality of fiberglass/unsaturated polyester composite panels. Polymer Composites, 2011, 32(9): 1473-80.

[2] Konstantopoulos, S., Grössing, H., Hergan, P., Weninger, M. and Schledjewski, R. (2018), Determination of the unsaturated through-thickness permeability of fibrous preforms based on flow front detection by ultrasound. Polym. Compos., 39: 360-367.

[3] Ouagne, P., Ouahbi, T., Park, C. H., Bréard, J., & Saouab, A. Continuous measurement of fiber reinforcement permeability in the thickness direction: Experimental technique and validation. Composites Part B: Engineering, 2013, 45(1): 609-618.

[4] May, D., Aktas, A., Advani, S. G., Berg, D. C., Endruweit, A., Fauster, E., ... & Ziegmann, G. In-plane permeability characterization of engineering textiles based on radial flow experiments: A benchmark exercise. Composites Part A: Applied Science and Manufacturing, 2019, 121: 100-114.

[5] ISO (2021). 4410 Experimental characterization of in-plane permeability of fibrous reinforcements for liquid composite moulding. https://www.iso.org/standard/79944.html.

[6] Weitzenböck J R, Shenoi R A, Wilson P A. Radial flow permeability measurement. Part A: Theory. Composites Part A: Applied Science and Manufacturing, 1999, 30(6): 781-796.

[7] Weitzenböck J R, Shenoi R A, Wilson P A. Radial flow permeability measurement. Part B: Application. Composites Part A: applied science and manufacturing, 1999, 30(6): 797-813.

[8] Yong, A. X. H., Aktas, A., May, D., Endruweit, A., Advani, S., Hubert, P., ... & Willenbacher, B. Out-of-plane permeability measurement for reinforcement textiles: A benchmark exercise. Composites Part A: Applied Science and Manufacturing, 2021, 148: 106480.

[9] Nedanov P B, Advani S G. A method to determine 3D permeability of fibrous reinforcements. Journal of composite materials, 2002, 36(2): 241-254.

[10] Yun, M., Sas, H., Simacek, P., & Advani, S. G. Characterization of 3D fabric permeability with skew terms. Composites Part A: Applied Science and Manufacturing, 2017, 97: 51-59.

[11] Stöven, T., Weyrauch, F., Mitschang, P., & Neitzel, M. Continuous monitoring of three-dimensional resin flow through a fibre preform. Composites Part A: Applied Science and Manufacturing, 2003, 34(6): 475-480.

[12] Becker, D., Grössing, H., Konstantopoulos, S., Fauster, E., Mitschang, P., & Schledjewski, R. An evaluation of the reproducibility of ultrasonic sensor-based out-of-plane permeability measurements: a benchmarking study. Advanced Manufacturing: Polymer & Composites Science, 2016, 2(1): 34-45.

[13] Konstantopoulos, S., Grössing, H., Hergan, P., Weninger, M., & Schledjewski, R. Determination of the unsaturated through-thickness permeability of fibrous preforms

based on flow front detection by ultrasound. Polymer Composites, 2018, 39(2): 360-367.

[14] Weitzenböck J R, Shenoi R A, Wilson P A. Measurement of three-dimensional permeability. Composites Part A: Applied Science and Manufacturing, 1998, 29(1-2): 159-169.

[15] Antonucci, V., Giordano, M., Nicolais, L., Calabro, A., Cusano, A., Cutolo, A., & Inserra, S. Resin flow monitoring in resin film infusion process. Journal of Materials Processing Technology, 2003, 143: 687-692.

[16] Ahn S H, Lee W I, Springer G S. Measurement of the three-dimensional permeability of fiber preforms using embedded fiber optic sensors. Journal of Composite Materials, 1995, 29(6): 714-733.

[17] Lim S T, Lee W I. An analysis of the three-dimensional resin-transfer mold filling process. Composites Science and Technology, 2000, 60(7): 961-975.

[18] Mekic S, Akhatov I, Ulven C. A radial infusion model for transverse permeability measurements of fiber reinforcement in composite materials. Polymer Composite, 2009;30:907–17.

[19] Pedro S, Stepan V. L, Jan I. Methodology of dry and wet compressibility measurement - ScienceDirect. Composites Part A: Applied Science and Manufacturing, 128.

[20] Chen X, Papathanasiou T D. On the variability of the Kozeny constant for saturated flow across unidirectional disordered fiber arrays. Composites Part A: Applied Science and Manufacturing, 2006, 37(6): 836-846.